Journal of Computational Physics 332 (2017) 83–98

Contents lists available at ScienceDirect

Journal of Computational Physics

www.elsevier.com/locate/jcp

Spectral-collocation variational integrators

Yiqun Li [a,*], Boying Wu [a], Melvin Leok [b]

[a] Department of Mathematics, Harbin Institute of Technology, Harbin 150001, PR China
[b] Department of Mathematics, University of California at San Diego, La Jolla, CA 92093, USA

ARTICLE INFO

Article history:
Received 30 July 2015
Received in revised form 3 December 2016
Accepted 3 December 2016
Available online 8 December 2016

Keywords:
Geometric numerical integration
Variational integrators
Spectral-collocation methods
Lagrangian mechanics

ABSTRACT

Spectral methods are a popular choice for constructing numerical approximations for smooth problems, as they can achieve geometric rates of convergence and have a relatively small memory footprint. In this paper, we introduce a general framework to convert a spectral-collocation method into a shooting-based variational integrator for Hamiltonian systems. We also compare the proposed spectral-collocation variational integrators to spectral-collocation methods and Galerkin spectral variational integrators in terms of their ability to reproduce accurate trajectories in configuration and phase space, their ability to conserve momentum and energy, as well as the relative computational efficiency of these methods when applied to some classical Hamiltonian systems. In particular, we note that spectrally-accurate variational integrators, such as the Galerkin spectral variational integrators and the spectral-collocation variational integrators, combine the computational efficiency of spectral methods together with the geometric structure-preserving and long-time structural stability properties of symplectic integrators.

1. Introduction

Symplectic integrators have long played an important role in the long-time simulation of mechanical systems [2,3], and the characterization of symplectic integrators in terms of variational integrators [16] has proven to be very fruitful. Additionally, variational integrators can be applied to the discretization of optimal control problems in robotics and aeronautics [7,10,11,21]. The basic idea of a variational integrator is to construct the numerical scheme by discretizing the appropriate variational principle, e.g., Hamilton's principle for conservative systems, and the Lagrange–d'Alembert principle for dissipative or forced systems. The resulting integrators exhibit clear advantages when compared with conventional numerical integration algorithms. They are symplectic, momentum-preserving, and exhibit near energy conservation for exponentially long times. Moreover, they can be easily extended to a large class of problems, such as Lagrangian and Hamiltonian PDEs [14], Lie–Poisson dynamical systems [17], and optimal control problems [10,21]. A comparison of spectral-collocation methods and symplectic methods when applied to Hamiltonian systems was conducted in [8], and in this paper, we will discuss methods for constructing spectrally-accurate variational integrators that combine the geometric convergence of spectral methods and the geometric structure-preserving properties of symplectic integrators.

There are two general methods for constructing higher-order variational integrators, the first is the Galerkin construction [13,18], and the other is the shooting-based construction [12,19]. The construction of Galerkin variational integrators relies on a variational characterization of the exact discrete Lagrangian, which is then approximated through the choice of a

* Corresponding author.
E-mail addresses: liyiqun_hit@163.com (Y. Li), mathwby@hit.edu.cn (B. Wu), mleok@math.ucsd.edu (M. Leok).

http://dx.doi.org/10.1016/j.jcp.2016.12.007
0021-9991/

finite-dimensional function space and a sufficiently accurate quadrature formula. The shooting-based approach relies on the characterization of the exact discrete Lagrangian in terms of Jacobi's solution of the Hamilton–Jacobi equation, which involves evaluating the action integral on the solution of the Euler–Lagrange boundary value problem. This is approximated by constructing a numerical approximation of the solution of the Euler–Lagrange boundary value problem by using the shooting method and approximating the action integral with a numerical quadrature formula.

In this paper, we first present a brief overview of Lagrangian and Hamiltonian mechanics and variational integrators in Section 1. In Section 2, we introduce the construction and convergence analysis of shooting-based variational integrators derived from spectral-collocation methods. In Section 3, practical numerical algorithms for implementing spectral-collocation variational integrators are presented, and numerical examples are given in Section 4. In Section 5, we make some concluding remarks and comment on possible future directions.

1.1. Lagrangian and Hamiltonian mechanics

Lagrangian mechanics Consider a mechanical system on an n-dimensional configuration manifold Q with generalized coordinates $q^i, i = 1, ..., n$, which is described by a Lagrangian $L : TQ \to \mathbb{R}$ that is given by the kinetic energy minus the potential energy. The action $\mathfrak{S} : C^2([a, b], Q) \to \mathbb{R}$ is given by

$$\mathfrak{S}(q) = \int_a^b L(q, \dot{q})dt.$$

Then, Hamilton's principle states that the action is stationary for curves $q \in C^2([a, b], Q)$ with fixed endpoints, i.e.,

$$\delta\mathfrak{S}(q) = \delta \int_a^b L(q, \dot{q})dt = 0, \tag{1}$$

where $\delta q(a) = \delta q(b) = 0$. By the fundamental theorem of the calculus of variations, we have

$$\frac{d}{dt}\frac{\partial L}{\partial \dot{q}^i} - \frac{\partial L}{\partial q^i} = 0, \tag{2}$$

which are referred to as the Euler–Lagrange equations.

Hamiltonian mechanics Alternatively, the mechanical system can be described by a Hamiltonian $H : T^*Q \to \mathbb{R}$ given by

$$H(q, p) = p_i\dot{q}^i - L(q, \dot{q}),$$

where the velocities on the right-hand side are implicitly defined in terms of the momenta by the Legendre transformation $p_i = \frac{\partial L}{\partial \dot{q}^i}$, and there is an implicit summation over the index i. This leads to Hamilton's principle in phase space,

$$\delta \int [p_i\dot{q}^i - H(q, p)]dt = 0,$$

where we again assume that the variations in q vanish at the endpoints, i.e., $\delta q(a) = \delta q(b) = 0$. By the fundamental theorem of the calculus of variations,

$$\dot{q}^i = \frac{\partial H}{\partial p_i}, \qquad \dot{p}_i = -\frac{\partial H}{\partial q^i}, \qquad i = 1, \ldots, n, \tag{3}$$

which are Hamilton's canonical equations.

1.2. Discrete mechanics and variational integrators

Discrete Lagrangian mechanics [16] is based on a discrete analogue of Hamilton's principle. We first consider a discrete Lagrangian, $L_d : Q \times Q \to \mathbb{R}$, and construct the discrete action sum, $\mathfrak{S}_d : Q^{n+1} \to \mathbb{R}$, which is given by

$$\mathfrak{S}_d(q_0, q_1, ..., q_n) = \sum_{i=0}^{n-1} L_d(q_i, q_{i+1}).$$

Then, the discrete Hamilton's principle states that

$$\delta\mathfrak{S}_d = 0$$

for variations that vanish at the endpoints, i.e., $\delta q_0 = \delta q_n = 0$. This yields the discrete Euler–Lagrange (DEL) equation,

$$D_2L_d(q_{k-1},q_k)+D_1L_d(q_k,q_{k+1})=0,\qquad k=1,2,\cdots,n-1, \tag{4}$$

which implicitly defines the discrete Lagrangian map $F_{L_d}:(q_{k-1},q_k)\mapsto(q_k,q_{k+1})$. Here, D_1 and D_2 denote partial derivatives with respect to the first and second variables, respectively. This is equivalent to the implicit discrete Euler–Lagrange (IDEL) equations,

$$p_k=-D_1L_d(q_k,q_{k+1}),\qquad p_{k+1}=D_2L_d(q_k,q_{k+1}),\qquad k=0,1,\cdots,n-1, \tag{5}$$

which implicitly define the discrete Hamiltonian map $\tilde{F}_{L_d}:(q_k,p_k)\mapsto(q_{k+1},p_{k+1})$ where the discrete Lagrangian can be viewed as the Type I generating function of a symplectic transformation. The discrete Lagrangian and Hamiltonian maps describe numerical integration schemes that are referred to as variational integrators, and they are automatically symplectic and exhibit excellent long-time energy behavior. If the discrete Lagrangian is invariant under the diagonal action of a symmetry group, then there is a discrete momentum map that is preserved via a discrete version of Noether's theorem.

As we observed, the discrete Lagrangian, $L_d:Q\times Q\to\mathbb{R}$, is a generating function of a symplectic flow. Furthermore, there exists a generating function that generates the exact time-h flow map of Hamilton's equations, which we refer to as the exact discrete Lagrangian,

$$L_d^E(q_k,q_{k+1})=\int_{t_k}^{t_{k+1}}L(q_{k,k+1}(t),\dot{q}_{k,k+1}(t))dt, \tag{6}$$

where $q_{k,k+1}(t_k)=q_k$, $q_{k,k+1}(t_{k+1})=q_{k+1}$ and $q_{k,k+1}$ satisfies the Euler–Lagrange equation in the time interval $[t_k,t_{k+1}]$. The exact discrete Lagrangian is related to Jacobi's solution of the Hamilton–Jacobi equation. Alternatively, one can characterize the exact discrete Lagrangian variationally as follows,

$$L_d^E(q_k,q_{k+1};h)=\operatorname*{ext}_{\substack{q\in C^2([kh,(k+1)h],Q)\\ q(kh)=q_k,q((k+1)h)=q_{k+1}}}\int_{t_k}^{t_{k+1}}L(q(t),\dot{q}(t))dt. \tag{7}$$

In Section 2.3 of [16], the concept of variational error analysis is introduced. Essentially, it states that if one can construct a computable approximation of the exact discrete Lagrangian to a given order of accuracy, then it generates a numerical one-step method via the discrete Hamiltonian map with the same order of accuracy.

An alternative way of describing the discrete Lagrangian and Hamiltonian maps is in terms of the discrete Legendre transforms, $\mathbb{F}^{\pm}L_d:Q\times Q\to T^*Q$, that were introduced in [16],

$$\mathbb{F}^+L_d:(q_k,q_{k+1})\mapsto(q_{k+1},p_{k+1})=(q_{k+1},D_2L_d(q_k,q_{k+1})),$$
$$\mathbb{F}^-L_d:(q_k,q_{k+1})\mapsto(q_k,p_k)=(q_k,-D_1L_d(q_k,q_{k+1})).$$

Given these definitions, we can introduce the following commutative diagram, which shows the relationship between the discrete Lagrangian map, the discrete Hamiltonian map and the discrete Legendre transformations,

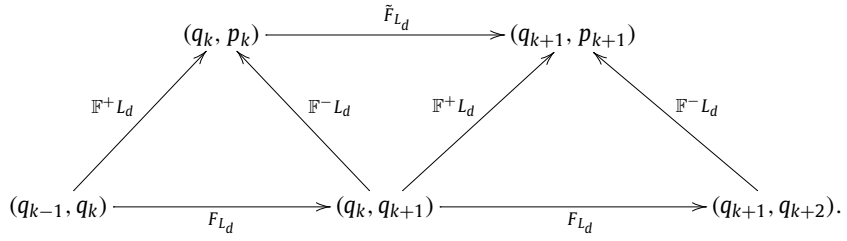

It is clear that the discrete Hamiltonian map can be described as $\tilde{F}_{L_d}=\mathbb{F}^+L_d\circ(\mathbb{F}^-L_d)^{-1}$, and the discrete Lagrangian map $F_{L_d}=(\mathbb{F}^-L_d)^{-1}\circ\mathbb{F}^+L_d$.

2. Shooting-based variational integrators from spectral-collocation methods

Spectral-collocation methods are well-known for their higher accuracy and geometric rates of convergence. Variational integrators are noted for their structure-preserving properties. Our aim in this section is to construct a spectral-collocation variational integrator (SCVI) that combines the benefits of these two numerical methods. To be specific, we discuss how one can construct a variational integrator that is based on a spectral-collocation method, that will achieve geometric rates of convergence under s refinement (s denotes the number of the collocation points in each time step). It should be noted that in this paper we will restrict our attention to configuration spaces Q that are vector spaces. A generalization of spectral-collocation variational integrators for mechanical systems on Lie groups will be described in future work.

2.1. Construction of spectral-collocation variational integrators

2.1.1. Outline of approach

The proposed approach is based on constructing an approximation of the exact discrete Lagrangian given in (6), which is given in terms of the action integral evaluated on the solution of the Euler–Lagrange boundary value problem. This was the approach taken in the shooting-based variational integrator that was introduced in [12], but in order to get high order of accuracy, one needed to have numerous quadrature points. Since this approach did not assume that the one-step method used to construct the variational integrator yielded a piecewise continuous approximation of the solution in the interior of the time interval, the approximations at the quadrature points were obtained by repeatedly applying the underlying one-step method.

In this section, we use the fact that a spectral-collocation method provides a continuous approximation of the solution of the Euler–Lagrange boundary value problem in the interior of the time interval, so we can use that to construct our computable discrete Lagrangian, and thereby reduce the computational burden of constructing higher-order shooting-based variational integrators.

2.1.2. Spectral-collocation discrete Lagrangian

Given a spectral-collocation method $\Psi_h^{(s)} : TQ \to TQ$ and a numerical quadrature formula

$$\int_0^h f(x)dx \approx h \sum_{i=1}^{m} w_i f(\tau_i h),$$

with quadrature weights w_i and quadrature nodes

$$0 \leq \tau_1 < \ldots < \tau_m \leq 1,$$

we construct the spectral-collocation discrete Lagrangian as follows:

$$L_d(q_0, q_1; h) = h \sum_{i=1}^{m} w_i L\left(\sum_{\nu=0}^{s} q_0^\nu \phi_\nu(\tau_i h), \sum_{\nu=0}^{s} q_0^\nu \dot{\phi}_\nu(\tau_i h) \right),$$

where $\{\phi_\nu\}_{\nu=0}^s \subset C^2([0,h],\mathbb{R})$ is a chosen set of basis functions, and $\{q_0^\nu\}_{\nu=1}^s \subset Q$ are obtained from the given spectral-collocation solution of the Euler–Lagrange boundary value problem. The spectral-collocation solution of the Euler–Lagrange boundary value problem is defined in two stages, we first solve for the $\tilde{v}_0$ that satisfies $\pi_Q \circ \Psi_h^{(s)}(q_0, \tilde{v}_0) = q_1$, then the $\{q_0^\nu\}_{\nu=1}^s$ are chosen so $\sum_{\nu=0}^s q_0^\nu \phi_\nu(t)$ is consistent with the initial condition $(q_0, \tilde{v}_0)$ and satisfies the Euler–Lagrange second-order differential equation at the collocation points. Here, $\pi_Q : TQ \to Q$ denotes the canonical projection and we use superscripts to index the value of q at the collocation points in the interval $[0,h]$.

2.2. Order of accuracy of the spectral-collocation discrete Lagrangian

For mechanical systems, the Euler–Lagrange equation is generally a second-order nonlinear differential equation, and it is a standard result in the numerical analysis of the shooting method for nonlinear problems [9] that the approximation error in the solution of a boundary value problem is bounded by the sum of two terms:

(i) the global error of the spectral-collocation method applied to the initial value problem;
(ii) the error associated with the rate of convergence of the nonlinear solver.

The order analysis of the shooting-based discrete Lagrangian depends mainly on the global approximation properties of the shooting solution of two-point boundary value problems and the accuracy of the quadrature formula. The analysis of h refinement for shooting-based variational integrators was developed in Theorem 1 of [12], which we state here.

Theorem 2.1. (Theorem 1 of [12]) *Given a p-th order accurate one-step method Ψ, a q-th order accurate quadrature formula, and a Lagrangian L that is Lipschitz continuous in both variables, the associated shooting-based discrete Lagrangian has order of accuracy* $\min(p,q)$.

This, together with Theorem 2.3.1 of [16], which is the basis of variational error analysis, establishes that the order of accuracy of the variational integrator generated by a shooting-based discrete Lagrangian is $\min(p,q)$.

2.3. Geometric convergence of the spectral-collocation discrete Lagrangian

We now prove that the shooting-based variational integrator based on spectral-collocation is geometrically convergent. We first cite Theorem 3.2 of [5] which extends variational error analysis to the case of geometric convergence of variational integrators.

Theorem 2.2. (Theorem 3.2 of [5]) *Given a regular Lagrangian L and corresponding Hamiltonian H, the following are equivalent for a discrete Lagrangian $L_d^{(s)}(q_0, q_1)$:*

(1) *there exists a positive constant K, where $K < 1$, such that the discrete Hamiltonian map for $L_d^{(s)}(q_0, q_h)$ has error $\mathcal{O}(K^s)$,*
(2) *there exists a positive constant K, where $K < 1$, such that the discrete Legendre transforms of $L_d^{(s)}(q_0, q_h)$ have error $\mathcal{O}(K^s)$,*
(3) *there exists a positive constant K, where $K < 1$, such that $L_d^{(s)}(q_0, q_h)$ approximates the exact discrete Lagrangian $L_d^E(q_0, q_h)$ with error $\mathcal{O}(K^s)$.*

With this result in mind, we state a theorem about the extent to which a spectral-collocation discrete Lagrangian approximates the exact discrete Lagrangian.

Theorem 2.3. *Given a sequence of spectral-collocation methods $\Psi_h^{(s)}$ with error bounded by $C_A K_A^s$ for some constants C_A, $K_A < 1$ that are independent of s and a sequence of quadrature rules $\mathcal{G}_s(f) = \sum_{j=1}^{m_s} b_{s_j} f(c_{s_j} h) \approx \int_0^h f(t)dt$, such that the quadrature error is bounded by $C_g K_g^s$ for some constants C_g, $K_g < 1$ that are independent of s and a Lagrangian L that is Lipschitz continuous in both variables, the associated spectral-collocation discrete Lagrangian $L_d^{(s)}$ has an error bounded by CK^s for some constants $C = (C_g + hK_L C_A)$, $K = \max(K_g, K_A) < 1$ that are independent of s.*

Proof. A converged shooting solution $(\tilde{q}_{k,k+1}, \tilde{v}_{k,k+1})$, associated with a geometrically convergent spectral-collocation method $\Psi_h^{(s)}$, approximates the exact solution $(q_{k,k+1}, v_{k,k+1})$ of the Euler–Lagrange boundary value problem with the following global error:

$$\|q_{k,k+1}(d_i) - \tilde{q}_{k,k+1}(d_i)\| \leq C_A K_A^s, \qquad \|v_{k,k+1}(d_i) - \tilde{v}_{k,k+1}(d_i)\| \leq C_A K_A^s$$

If the numerical quadrature formula is geometrically convergent, then

$$\begin{aligned}
&\|L_d^E(q_k, q_{k+1}) - L_d^{(s)}(q_k, q_{k+1})\| \\
&\quad = \left\| \int_{kh}^{(k+1)h} L(q_{k,k+1}(t), v_{k,k+1}(t))dt - h\sum_{j=1}^{m_s} b_{s_j} L(q_{k,k+1}(d_i), v_{k,k+1}(d_i)) \right. \\
&\qquad \left. + h\sum_{j=1}^{m_s} b_{s_j} L(q_{k,k+1}(d_i), v_{k,k+1}(d_i)) - h\sum_{j=1}^{m_s} b_{s_j} L(\tilde{q}_{k,k+1}(d_i), \tilde{v}_{k,k+1}(d_i)) \right\| \\
&\quad \leq \left\| \int_{kh}^{(k+1)h} L(q_{k,k+1}(t), v_{k,k+1}(t))dt - h\sum_{j=1}^{m_s} b_{s_j} L(q_{k,k+1}(d_i), v_{k,k+1}(d_i)) \right\| \\
&\qquad + \left\| h\sum_{j=1}^{m_s} b_{s_j} L(q_{k,k+1}(d_i), v_{k,k+1}(d_i)) - h\sum_{j=1}^{m_s} b_{s_j} L(\tilde{q}_{k,k+1}(d_i), \tilde{v}_{k,k+1}(d_i)) \right\| \\
&\quad \leq C_g K_g^s + h\sum_{j=1}^{m_s} b_{s_j} \left\| L(q_{k,k+1}(d_i), v_{k,k+1}(d_i)) - L(\tilde{q}_{k,k+1}(d_i), \tilde{v}_{k,k+1}(d_i)) \right\| \\
&\quad \leq C_g K_g^s + h\sum_{j=1}^{m_s} b_{s_j} K_L C_A K_A^s \\
&\quad = C_g K_g^s + hK_L C_A K_A^s \\
&\quad \leq (C_g + hK_L C_A) K^s
\end{aligned}$$

where $K = \max(K_g, K_A)$, and we used the quadrature error, consistency of the quadrature rule, the error estimates on the shooting solution, and the assumption that L is Lipschitz continuous with Lipschitz constant K_L. □

3. Implementation details

In this section, we describe the numerical implementation of a spectral-collocation variational integrator for mechanical systems with Lagrangian $L : TQ \to \mathbb{R}$. To approximate the trajectory $q : [0, T] \to Q$, we divide the total time interval $[0, T]$ into N subintervals of equal length h, a discrete curve in Q is defined in terms of piecewise polynomial curves $q : [kh, (k+1)h] \to Q$, $k = 0, ..., N-1$, that are subordinate to the partitioning of the time interval,

$$[0, T] = \bigcup_{k=0}^{N-1} [kh, (k+1)h], \quad N = T/h.$$

3.1. The choice of the spectral-collocation method and the quadrature rule

To construct a spectral-collocation variational integrator, we should choose a spectral-collocation method, a quadrature rule and a set of basis functions. In this paper, the implementation is mainly based on the Chebyshev collocation method, Gauss–Legendre quadrature and the basis functions $\phi_\nu(t) = l_\nu(t)$, where $l_\nu(t)$ are Lagrange interpolation polynomials based on the $s+1$ Chebyshev–Gauss–Lobatto points $c_j = \frac{(2k+1)h}{2} - \frac{h}{2}\cos(\frac{j\pi}{s})$, where c_j are the Chebyshev points $x_j = -\cos(\frac{j\pi}{s}), 0 \le j \le s$ rescaled from $[-1, 1]$ to $[kh, (k+1)h]$.

Besides the geometric convergence properties, the choice of Chebyshev collocation methods is motivated by the following considerations:

(1) Chebyshev collocation methods can be computed efficiently using the fast Fourier transform (FFT);
(2) the Chebyshev points include the boundary points (see Fig. 2) at kh and $(k+1)h$, and the use of Lagrange interpolants based on these points greatly simplify the computation of the discrete Legendre transforms $D_1L(q_k, q_{k+1})$ and $D_2L(q_k, q_{k+1})$;
(3) the Chebyshev spectral-collocation method is not symplectic. This is a desirable property, since our aim is to verify that the proposed shooting-based variational integrators provide a means of constructing symplectic methods out of non-symplectic spectral-collocation methods.

The choice of Gaussian quadrature is mainly because of the optimal accuracy. To be specific, an n-point Gaussian quadrature rule is exact for polynomials of degree $2n-1$. However, it is also possible to use other spectral-collocation methods and quadrature rules. For example, the trigonometric collocation methods might be a good choice for problems with oscillatory solutions. While we have primarily discussed numerical quadrature formulas that only depend on the integrand, one could consider more general quadrature formulas that depend on derivatives of the integrand, such as Gauss–Hermite quadrature. Different combinations of quadrature formulas and spectral-collocation methods may led to more effective integrators for specific classes of problems and we make no claim that the choices made in this paper are optimal.

3.2. Practical algorithms

In this section, we will first introduce the spectral-collocation method for the Euler–Lagrange equation, then we will derive the detailed expressions for the spectral-collocation variational integrator. As the Euler–Lagrange equation is generally a second-order nonlinear differential equation, we introduce the differentiation matrix approach to spectral-collocation methods based on the Chebyshev–Gauss–Lobatto points $\{c_j\}_{j=0}^s$ for the following second-order initial value problem,

$$\begin{cases} \ddot{q}(t) = f(t, q(t), \dot{q}(t)), \quad a < t \le b, \\ q(c_0) = q_0,\ \dot{q}(c_0) = v_0, \end{cases} \tag{8}$$

where

$$q(t) = [q_1(t), q_2(t), \cdots, q_M(t)],$$
$$f(t, q, \dot{q}) = [f_1(t, q, \dot{q}), f_2(t, q, \dot{q}), \cdots, f_M(t, q, \dot{q})].$$

By introducing the auxiliary variable $v(t) = \dot{q}(t)$, (8) can be converted to a system of first-order differential equations,

$$\begin{cases} \dot{q}(t) = v(t), \\ \dot{v}(t) = f(t, q(t), v(t)), \end{cases} \tag{9}$$

with initial conditions $q(c_0) = q_0,\ v(c_0) = \dot{q}_0$. Equation (9) can be discretized by introducing the first-order Chebyshev differentiation matrix $\tilde{A}$ in the interval $[a, b]$, which we will discuss in greater detail below, to obtain,

$$\tilde{A}\tilde{Q} = V, \tag{10}$$
$$\tilde{A}\tilde{V} = F(t, Q, V), \tag{11}$$

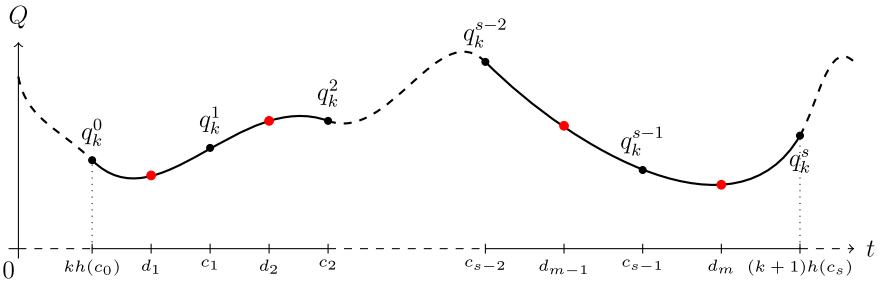

Fig. 1. The red dots represent the quadrature points, which may or may not be the same as the interpolation points which are represented by black dots. (For interpretation of the references to color in this figure legend, the reader is referred to the web version of this article.)

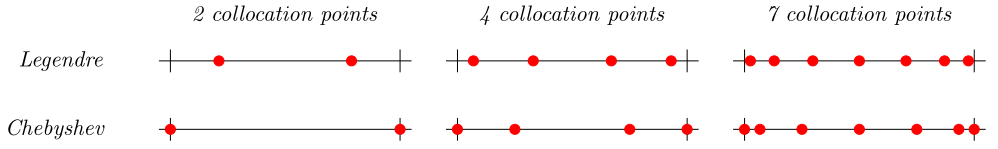

Fig. 2. Plots of Legendre–Gauss points and Chebyshev–Gauss–Lobatto points.

where

$$\tilde{Q} = [q_0, Q]^T,\ Q = [q(c_1), q(c_2), ..., q(c_s)]^T,$$
$$\tilde{V} = [v_0, V]^T,\ V = [v(c_1), v(c_2), ..., v(c_s)]^T,$$
$$F(t, Q, V) = [f(c_1, q(c_1), v(c_1)), f(c_2, q(c_2), v(c_2)), \ldots, f(c_s, q(c_s), v(c_s))]^T.$$

The first-order Chebyshev differentiation matrix $\tilde{A}$ in the interval $[a, b]$ is given by [15],

$$\tilde{A} = -\frac{2}{b-a} D^{(1)}(1:s, 0:s), \tag{12}$$

where $D^{(1)}$ is the $(s+1)\times(s+1)$ first-order Chebyshev differential matrix in the interval $[-1, 1]$ that is indexed from 0 to s and is given in [22] by

$$D^{(1)}_{i,j} = \begin{cases} \frac{2s^2+1}{6}, & i = j = 0, \\ \frac{-x_j}{2(1-x_j^2)}, & i = j = 1, ..., s-1, \\ \frac{\alpha_i(-1)^{(i+j)}}{\alpha_j(x_i - x_j)}, & i \neq j, i, j = 0, ..., s, \\ -\frac{2s^2+1}{6}, & i = j = s, \end{cases} \qquad \alpha_l = \begin{cases} 2, & l = 0 \text{ or } s, \\ 1, & \text{otherwise.} \end{cases} \tag{13}$$

As the initial value q_0 is given, we can partition the matrices into $\tilde{A} = [a_0, A]$ and $\tilde{Q} = [q_0, Q]^T$, which allows us to rewrite (10) and (11) in the following way,

$$AQ + a_0 q_0 = V, \tag{14}$$
$$AV + a_0 v_0 = F(t, Q, V). \tag{15}$$

Substituting (14) into (15), we obtain

$$A(AQ + a_0 q_0) + a_0 \dot{q}_0 = F(t, Q, AQ + a_0 q_0), \tag{16}$$

which is equivalent to the following nonlinear equation

$$A^2 \otimes I_M \mathrm{vec}(Q) = \mathrm{vec}(F(t, Q, AQ + a_0 q_0)) - a_0 \otimes \dot{q}_0^T - (Aa_0) \otimes q_0^T, \tag{17}$$

where I_M is the $M \times M$ identity matrix, and vec takes an $m \times n$ matrix and returns a vector of length mn by concatenating the columns of the matrix below each other. Then, $\mathrm{vec}(Q)$ can be obtained from (17) by using a nonlinear root finder.

Now, we can construct the spectral-collocation discrete Lagrangian based on the chosen Chebyshev–Lagrange interpolation and Gauss–Legendre quadrature. For an arbitrary interval $[kh, (k+1)h]$ (see Fig. 1), we can approximate the value of q and $\dot{q}$ at the quadrature points by:

$$q(d_i;q_k^\nu,h)=\sum_{\nu=0}^{s}q_k^\nu l_{\nu,s}(\tau(d_i)),\qquad \dot q(d_i;q_k^\nu,h)=\sum_{\nu=0}^{s}q_k^\nu \dot l_{\nu,s}(\tau(d_i))\frac{\mathrm{d}\tau}{\mathrm{d}t}=\frac{2}{h}\sum_{\nu=0}^{s}q_k^\nu \dot l_{\nu,s}(\tau(d_i)),$$

where $q_k^\nu=q_k(c_\nu)$ and $\tau(t)=\frac{2}{h}(t-t_k)-1\in[-1,1]$, d_i are the quadrature points in the interval $[t_k,t_{k+1}]$, and $l_{\nu,s}:[-1,1]\to\mathbb{R}$ are the Lagrange polynomials of degree s that are given by

$$l_{\nu,s}(\tau)=\prod_{0\le j\le s,\, j\neq\nu}\frac{\tau-x_j}{x_\nu-x_j}.$$

Then, the spectral-collocation discrete Lagrangian is given by

$$\begin{aligned}L_d(q_k=q_k^0,q_k^1,\ldots,q_k^s=q_{k+1};h)&=\frac{h}{2}\sum_{i=1}^{m}w_i L(q(d_i;q_k^\nu,h),\dot q(d_i;q_k^\nu,h))\\&=\frac{h}{2}\sum_{i=1}^{m}w_i L\left(\sum_{\nu=0}^{s}q_k^\nu l_{\nu,s}(\tau(d_i)),\frac{2}{h}\sum_{\nu=0}^{s}q_k^\nu \dot l_{\nu,s}(\tau(d_i))\right),\end{aligned}\tag{18}$$

where $\{q_k^\nu\}_{\nu=0}^s$ are obtained by solving the Euler–Lagrange boundary value problem using the spectral-collocation method (17). In practice, we explicitly compute the implicit discrete Euler–Lagrange equations (5),

$$p_k=-D_1L_d(q_k,q_{k+1};h),\qquad p_{k+1}=D_2L_d(q_k,q_{k+1};h)$$

for the discrete Lagrangian given by (18), and combine it with the spectral-collocation method (17) to yield a set of nonlinear equations,

$$A^2\otimes I_M\,\mathrm{vec}(Q)=\mathrm{vec}(F(Q,AQ+a_0q_k^0))-a_0\otimes(v_k^0)^T-(Aa_0)\otimes(q_k^0)^T,\tag{19a}$$

$$q_k^0=q_k,\tag{19b}$$

$$q_k^s=q_{k+1}^0=q_{k+1},\tag{19c}$$

$$p_k=-\sum_{i=1}^{m}w_i\left[\frac{h}{2}l_{0,s}(\tau_i)\frac{\partial L}{\partial q}\Big(\sum_{\nu=0}^{s}q_k^\nu l_{\nu,s}(\tau_i),\frac{2}{h}\sum_{\nu=0}^{s}q_k^\nu \dot l_{\nu,s}(\tau_i)\Big)+\dot l_{0,s}(\tau_i)\frac{\partial L}{\partial\dot q}\Big(\sum_{\nu=0}^{s}q_k^\nu l_{\nu,s}(\tau_i),\frac{2}{h}\sum_{\nu=0}^{s}q_k^\nu \dot l_{\nu,s}(\tau_i)\Big)\right],\tag{19d}$$

$$p_{k+1}=\sum_{i=1}^{m}w_i\left[\frac{h}{2}l_{s,s}(\tau_i)\frac{\partial L}{\partial q}\Big(\sum_{\nu=0}^{s}q_k^\nu l_{\nu,s}(\tau_i),\frac{2}{h}\sum_{\nu=0}^{s}q_k^\nu \dot l_{\nu,s}(\tau_i)\Big)+\dot l_{s,s}(\tau_i)\frac{\partial L}{\partial\dot q}\Big(\sum_{\nu=0}^{s}q_k^\nu l_{\nu,s}(\tau_i),\frac{2}{h}\sum_{\nu=0}^{s}q_k^\nu \dot l_{\nu,s}(\tau_i)\Big)\right],\tag{19e}$$

where $Q=(q_k^1,q_k^2,\ldots,q_k^s)$. Given an initial condition (q_k,p_k), we can obtain $Q=(q_k^1,q_k^2,\ldots,q_k^s)$ by solving equations (19a), (19b) and (19d) with a nonlinear root finder, then (q_{k+1},p_{k+1}) can be obtained from (19c) and (19e). In this paper, we use the Newton method as the nonlinear solver. This procedure is summarized in the diagram below,

$$(q_k,p_k)\xrightarrow{(19a)(19b)(19d)}Q=(q_k^1,q_k^2,\ldots,q_k^s)\xrightarrow{(19c)(19e)}(q_{k+1},p_{k+1})$$
$$k\leftarrow k+1$$

and the iterative algorithm can be described as follows (see Algorithm 1),

Remark 3.1. Using the Legendre transformation, the above system of nonlinear equations can also be expressed in terms of the generalized coordinates and momenta (q,p) on the cotangent bundle T^*Q, and the Hamiltonian $H:T^*Q\to\mathbb{R}$, where $H(q,p)=p\dot q-L(q,\dot q)|_{p=\partial L/\partial\dot q}$. Using the definition of the Hamiltonian in terms of the Lagrangian, we conclude that $\frac{\partial H}{\partial q}(q,p)=-\frac{\partial L}{\partial q}(q,\dot q)=-\dot p$ and $\frac{\partial H}{\partial p}=\dot q$ (see page 380 of [16]), which yields the following equivalent system of equations expressed in terms of the Hamiltonian,

$$A^2\otimes I_M\,\mathrm{vec}(Q)=\mathrm{vec}(F(Q,AQ+a_0q_k^0))-a_0\otimes(v_k^0)^T-(Aa_0)\otimes(q_k^0)^T,\tag{20a}$$

$$q_k^0=q_k,\tag{20b}$$

$$q_{k+1}^0=q_{k+1},\tag{20c}$$

$$p_k=-\sum_{i=1}^{m}w_i\left[-\frac{h}{2}l_{0,s}(\tau_i)\frac{\partial H}{\partial q}\Big(\sum_{\nu=0}^{s}q_k^\nu l_{\nu,s}(\tau_i),p_k^i\Big)+p_k^i\dot l_{0,s}(\tau_i)\right],\tag{20d}$$

$$p_{k+1}=\sum_{i=1}^{m}w_i\left[-\frac{h}{2}l_{s,s}(\tau_i)\frac{\partial H}{\partial q}\Big(\sum_{\nu=0}^{s}q_k^\nu l_{\nu,s}(\tau_i),p_k^i\Big)+p_k^i\dot l_{s,s}(\tau_i)\right],\tag{20e}$$

$$\frac{\partial H}{\partial p}\Big(\sum_{\nu=0}^{s} q_k^{\nu} l_{\nu,s}(\tau_i),\, p_k^i\Big) - \frac{2}{h}\sum_{\nu=0}^{s} q_k^{\nu} \dot{l}_{\nu,s}(\tau_i) = 0, \qquad i = 1, ..., m, \tag{20f}$$

where the p_k^i are internal stages that approximate the momentum at time $t_k + \frac{h}{2}(\tau_i + 1)$.

4. Numerical examples

To verify the effectiveness of the proposed spectral-collocation variational integrator, we compute the solution of the planar pendulum and the Kepler two-body problem, where the nonlinear equations that define the method are solved using the Newton method, the error indicator is the maximum componentwise error,

$$\max(\|Q^{i+1} - Q^i\|_{\ell^\infty}, \|P^{i+1} - P^i\|_{\ell^\infty}),$$

the tolerance is chosen to be 10^{-12}, and the maximum iteration count is set to 1000. In practice, when the step sizes are sufficiently small, the Newton method typically converges in about 10 iterations or less, but if significantly larger step sizes are desired, then one might consider applying a trust-region method instead. The numerical experiments were carried out on a personal computer with an Intel Core i5-4210U, 1.70 GHz CPU, 8G RAM and the algorithms were implemented using Matlab 2014a.

4.1. Planar pendulum

In order to illustrate the structure of the algorithms presented in Section 3.2, we consider a simple illustrative example. The pendulum consists of a mass m attached on a rod of length l. Considering the planar motion in the x-z plane, where the generalized coordinate q lies on the one-sphere S^1 and denotes the angle that the rod makes with the direction of gravity. Then, the Lagrangian is given by,

$$L(q, \dot{q}) = \frac{ml^2\dot{q}^2}{2} + mgl\cos(q),$$

and the Hamiltonian is given by,

$$H(q, p) = \frac{p^2}{2ml^2} - mgl\cos(q).$$

The corresponding Euler–Lagrange equations are,

$$ml^2\ddot{q} + mgl\sin(q) = 0,$$

and Hamilton's equations are given by

$$\dot{q} = \frac{p}{ml^2}, \tag{21a}$$

$$\dot{p} = -mgl\sin(q), \quad (q, p) \in S^1 \times \mathbb{R}^1. \tag{21b}$$

For simplicity, we assume that $m = l = g = 1$. The equation has a center at $(0, 0)$ and saddle points at $(\pm\pi, 0)$. Here, we choose the two Chebyshev points $x_0 = -1$, $x_1 = 1$ as the collocation points, and the two-point Gauss quadrature formula $(w_i, \tau_i)_{i=1}^2$ for the interval $[-1, 1]$, where

$$w_i = 1; \quad \tau_i = \pm\frac{1}{\sqrt{3}}.$$

Then, the approximation of q is obtained by linear interpolation, and the values at the corresponding rescaled quadrature points in the interval $[kh, (k+1)h]$ are given by,

$$q(d_1) = l_{0,1}\Big(-\frac{1}{\sqrt{3}}\Big)q_k + l_{1,1}\Big(-\frac{1}{\sqrt{3}}\Big)q_{k+1} = \Big(\frac{3+\sqrt{3}}{6}\Big)q_k + \Big(\frac{3-\sqrt{3}}{6}\Big)q_{k+1}.$$

$$q(d_2) = l_{0,1}\Big(\frac{1}{\sqrt{3}}\Big)q_k + l_{1,1}\Big(\frac{1}{\sqrt{3}}\Big)q_{k+1} = \Big(\frac{3-\sqrt{3}}{6}\Big)q_k + \Big(\frac{3+\sqrt{3}}{6}\Big)q_{k+1}.$$

From (13), we can obtain the first-order Chebyshev differential matrix in the interval $[-1, 1]$ based on Chebyshev points $x_0 = -1$, $x_1 = 1$,

$$D^{(1)} = \begin{bmatrix} \frac{1}{2} & -\frac{1}{2} \\ \frac{1}{2} & -\frac{1}{2} \end{bmatrix}.$$

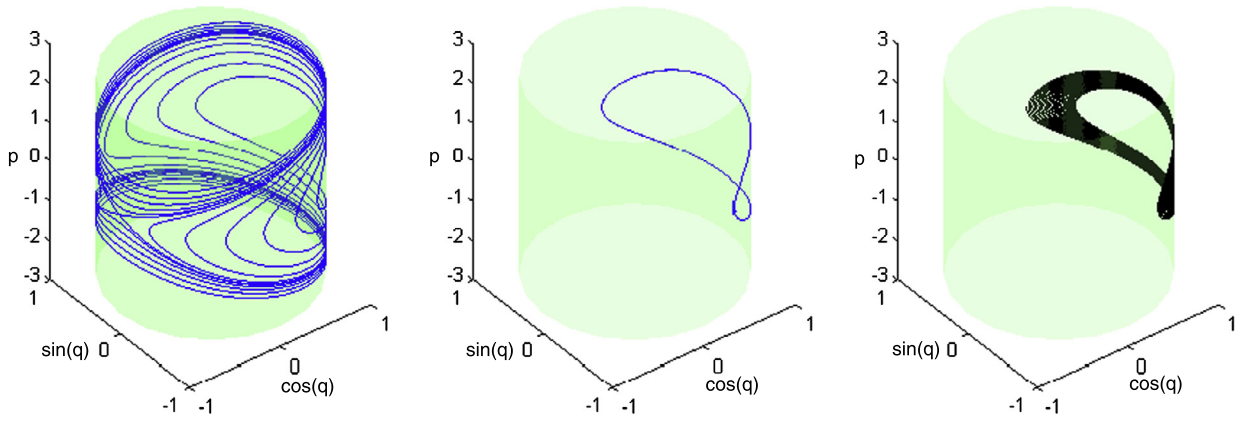

Fig. 3. Left: the phase portrait of the planar pendulum on the cylinder corresponding to a variety of initial conditions. Middle: the phase computed using SCVI with 2 point Chebyshev interpolation, 2 point Gauss–Legendre quadrature. Right: the phase computed using SC with 2 Chebyshev points. Step sizes are $h = 0.005$.

Then, the first-order Chebyshev differential matrix in the interval $[kh, (k+1)h]$ can be given by,

$$\tilde{A} = -\frac{2}{h} D^{(1)}\,(1:1, 0:1) = \left[-\frac{1}{h}, \frac{1}{h}\right].$$

We can partition the 1×2 matrix $\tilde{A}$ into $\tilde{A} = [a_0, A]$. Combined with (19b), (19a) has the form,

$$\frac{1}{h^2} q_{k+1} = -\sin(q_{k+1}) - \left(-\frac{1}{h}\right) v_k - \left(-\frac{1}{h^2}\right) q_k, \tag{22}$$

and (19d) can be obtain by direct calculation,

$$\lambda_k^1 q_k + \lambda_k^2 q_{k+1} + \beta_k + p_k = 0, \tag{23}$$

where

$$\Lambda_k = [\lambda_k^1, \lambda_k^2] = \left[\frac{2}{h}\sum_{i=1}^{2} w_i \dot{l}_{0,1}(\tau_i)\dot{l}_{0,1}(\tau_i), \frac{2}{h}\sum_{i=1}^{2} w_i \dot{l}_{0,1}(\tau_i)\dot{l}_{1,1}(\tau_i)\right] = \left[\frac{1}{h}, -\frac{1}{h}\right],$$

$$\beta_k = \frac{h}{2}\sum_{i=1}^{2} w_i l_{0,1}(\tau_i)\Big(-\sin\left(l_{0,1}(\tau_i)q_k + l_{1,1}(\tau_i)q_{k+1}\right)\Big)$$

$$= -\frac{(3+\sqrt{3})h}{12}\sin\left(\left(\frac{3+\sqrt{3}}{6}\right)q_k + \left(\frac{3-\sqrt{3}}{6}\right)q_{k+1}\right) - \frac{(3-\sqrt{3})h}{12}\sin\left(\left(\frac{3-\sqrt{3}}{6}\right)q_k + \left(\frac{3+\sqrt{3}}{6}\right)q_{k+1}\right).$$

So, we can solve for v_k and q_{k+1} using (22) and (23). Then, we can calculate p_{k+1} from (19e).

Choosing the initial condition $(q_0, p_0) = (0.5, 0)$, Fig. 3 compares the phase trajectories of the pendulum system, which are computed using the two-point spectral-collocation variational integrator (SCVI) constructed above and the spectral-collocation method (SC) also with two Chebyshev points. Fig. 4 shows the corresponding energy errors of these two methods. From the numerical results, we can see that SCVI preserves the phase space area and energy very well, as one would expect from a symplectic integrator, whereas the Chebyshev collocation method, which is non-symplectic, performs much more poorly in terms of preserving the phase area and energy. In particular, the Chebyshev collocation method exhibits a decay of the trajectory in phase space. Additionally, we see in Fig. 4 that the energy error for SC accumulates, whereas the energy error for SCVI remains bounded and small, which is consistent with the existence of a modified energy [20] that arises from backward error analysis when applying a symplectic integrator to a Hamiltonian system.

4.2. Kepler problem

The Kepler two-body problem describes the motion of two bodies under mutual gravitational attraction. If one body is placed at the origin, the corresponding Lagrangian and angular momentum of the Kepler two-body system are given by

$$L(q, v) = T - V = \frac{1}{2}(v_1^2 + v_2^2) - \frac{1}{\sqrt{q_1^2 + q_2^2}},$$

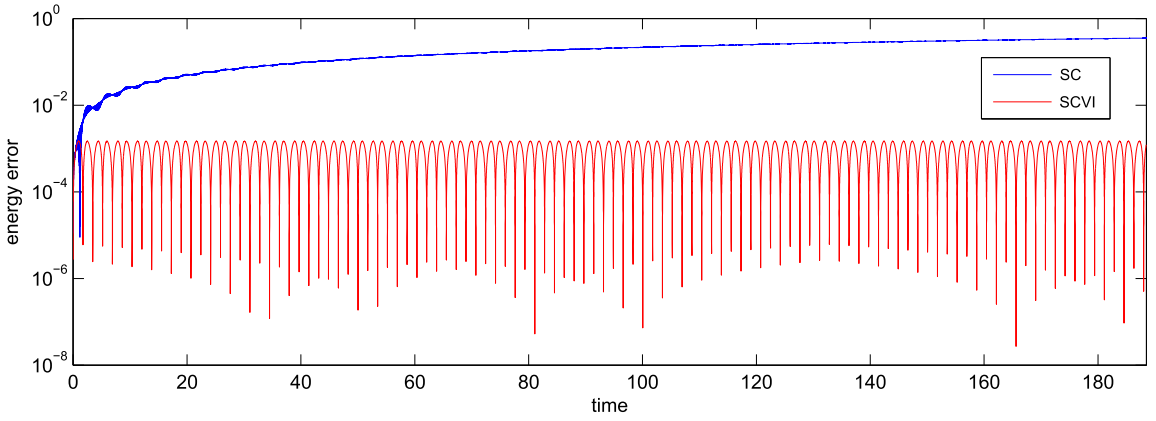

Fig. 4. Comparison of the energy error of the planar pendulum problem computed using SC with 2 Chebyshev points and SCVI with 2 point Chebyshev interpolation and 2 point Gauss–Legendre quadrature. Step sizes are $h = 0.005$. (For interpretation of the references to color in this figure, the reader is referred to the web version of this article.)

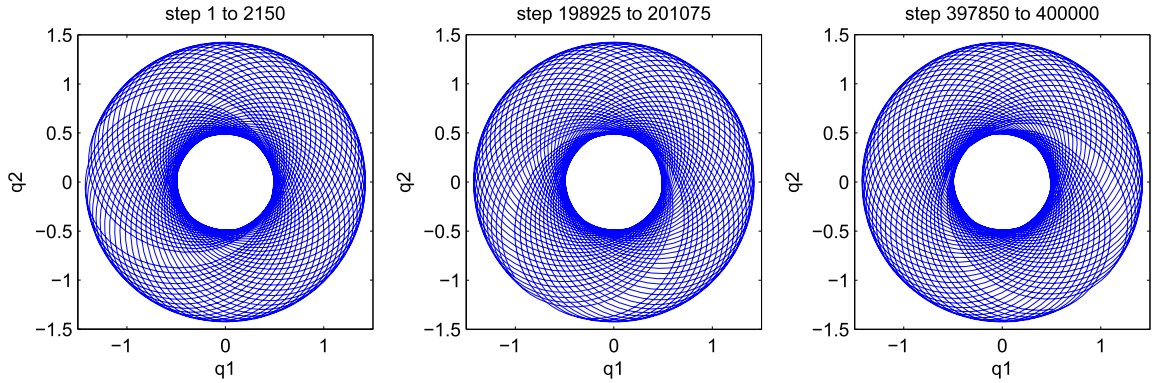

Fig. 5. Kepler two-body problem with eccentricity $e = 0.5$. Orbits computed using SCVI with 2 point Chebyshev interpolation, 4 point Gauss–Legendre quadrature. Step size $h = \pi/20$ and total time $T = 20000\pi$.

and

$$M(q, v) = q_1 v_2 - q_2 v_1,$$

respectively, where $q = (q_1, q_2)$ represents the position of the second body and $v = (v_1, v_2)$ represents the velocity. Using (2) we can easily obtain the Euler–Lagrange equations of the system,

$$\dot{q}_1 = v_1, \tag{24a}$$

$$\dot{q}_2 = v_2, \tag{24b}$$

$$\dot{v}_1 = -\frac{q_1}{(q_1^2 + q_2^2)^{3/2}}, \tag{24c}$$

$$\dot{v}_2 = -\frac{q_2}{(q_1^2 + q_2^2)^{3/2}}. \tag{24d}$$

For the system described by (24), given the eccentricity $0 \le e < 1$, we choose the following initial conditions,

$$q_1(0) = 1 - e, \quad q_2(0) = 0, \quad v_1(0) = 0, \quad v_2(0) = \sqrt{\frac{1+e}{1-e}},$$

which implies that $L_0 = -0.5$, $M_0 = \sqrt{1 - e^2}$. The period of the solution is 2π.

Fig. 5 shows the orbit of the Kepler problem when using SCVI with 2 point Chebyshev interpolation and 4 point Gauss–Legendre quadrature. We run the numerical program for 10000 periods. In order to maintain the visibility of the trajectory in the figure, we plot trajectory segments from the beginning, middle and end of the full trajectory. The numerical solution of (24) in the (q_1, q_2)-plane shows that the elliptical orbit of the second body is not distorted for long-time simulations. In particular, the eccentricity of the orbit remains unchanged even over 10000 periods, although the proposed method

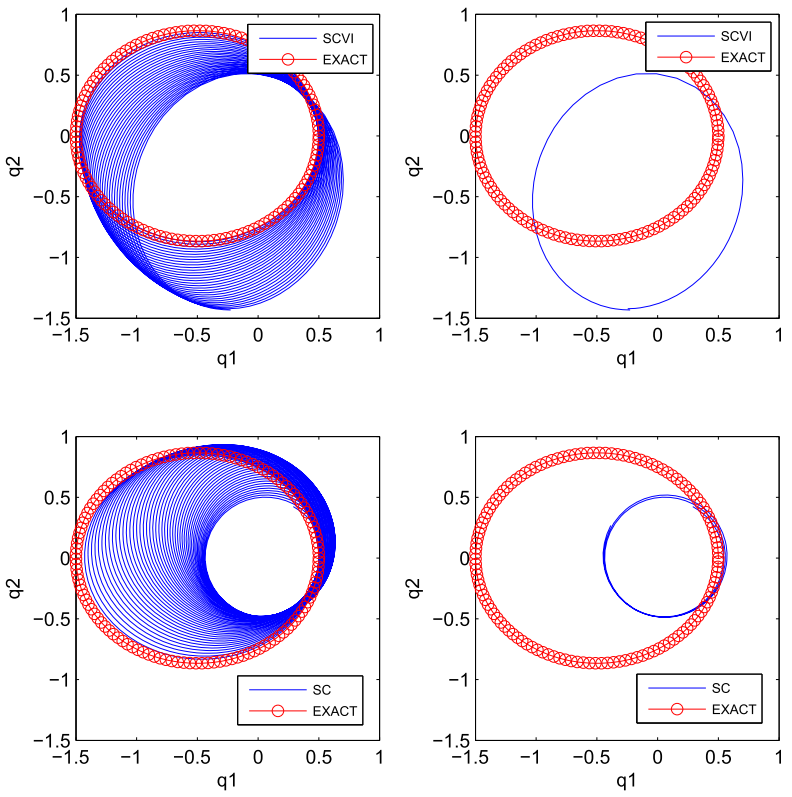

Fig. 6. Kepler two-body problem with eccentricity $e = 0.5$. Comparison of the orbit computed using SCVI with 2 point Chebyshev interpolation, 4 point Gauss–Legendre quadrature and SC with 3 Chebyshev points. Step sizes are $h = 0.1$ and total time $T = 60\pi$. The second column of figures show the last part of the trajectory for the duration of one orbital period.

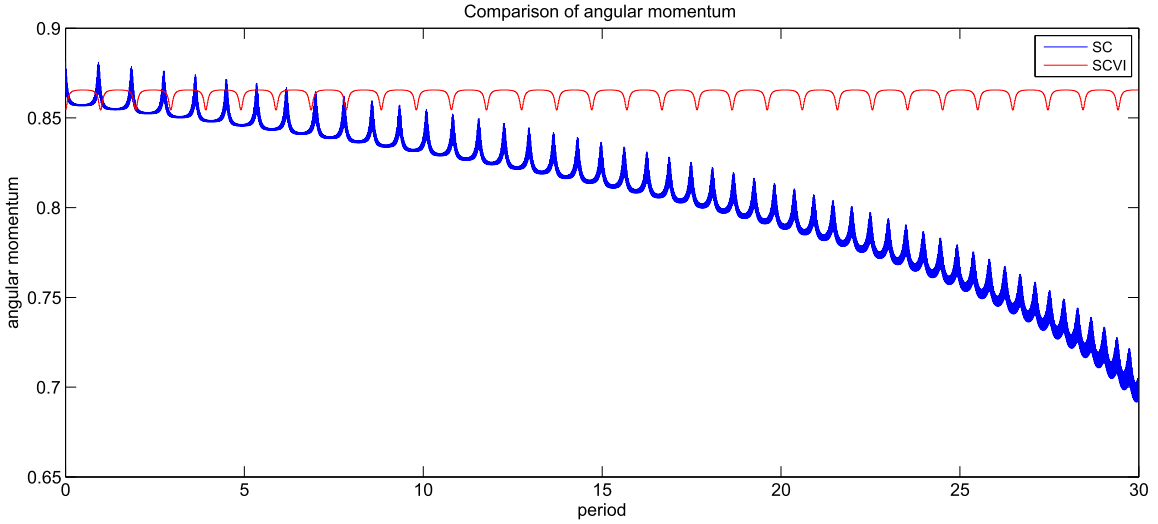

Fig. 7. Kepler two-body problem with eccentricity $e = 0.5$. Comparison of the angular momentum computed using SCVI with 2 point Chebyshev interpolation, 4 point Gauss–Legendre quadrature and SC with 3 Chebyshev points. Step sizes are $h = 0.1$ and total time $T = 60\pi$. (For interpretation of the references to color in this figure, the reader is referred to the web version of this article.)

does exhibit precession. To avoid the precession effect, one may choose a smaller step size or alternatively choose a larger number of interpolation points and quadrature points for SCVI (see Fig. 10).

In Figs. 6, 7 and 8, we compare the orbits, angular momenta and energies of the Kepler problem, which is simulated using SCVI with 2 point Chebyshev interpolation, 4 point Gauss–Legendre quadrature and Chebyshev collocation method with 3 collocation points (the two-point Chebyshev collocation method is not stable when we set the step size $h = 0.1$).

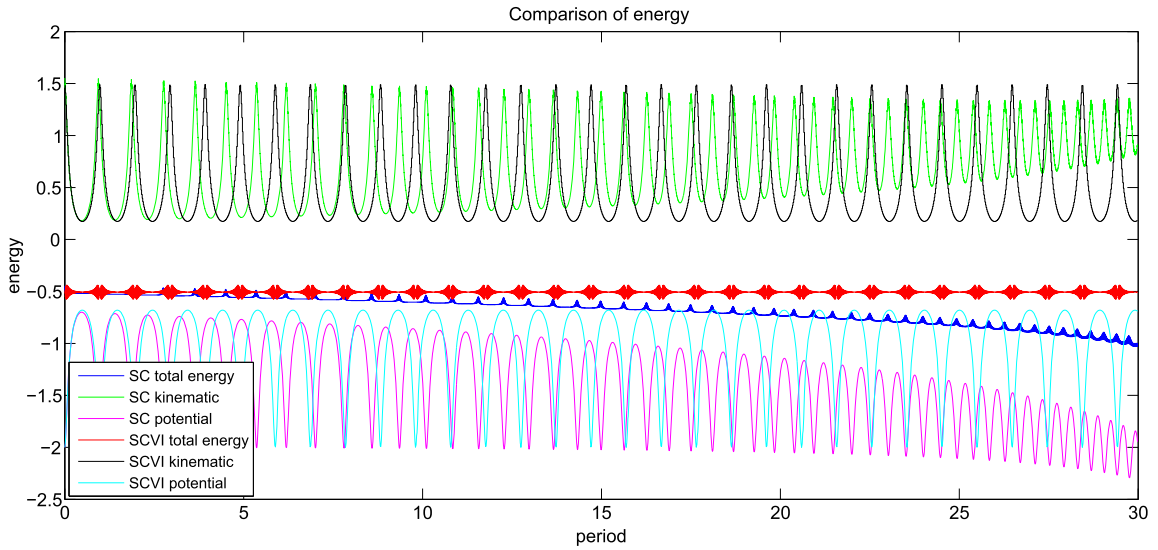

Fig. 8. Kepler two-body problem with eccentricity $e = 0.5$. Comparison of the energy computed using SCVI with 2 point Chebyshev interpolation, 4 point Gauss–Legendre quadrature and SC with 3 Chebyshev points. Step sizes are $h = 0.1$ and total time $T = 60\pi$. (For interpretation of the references to color in this figure, the reader is referred to the web version of this article.)

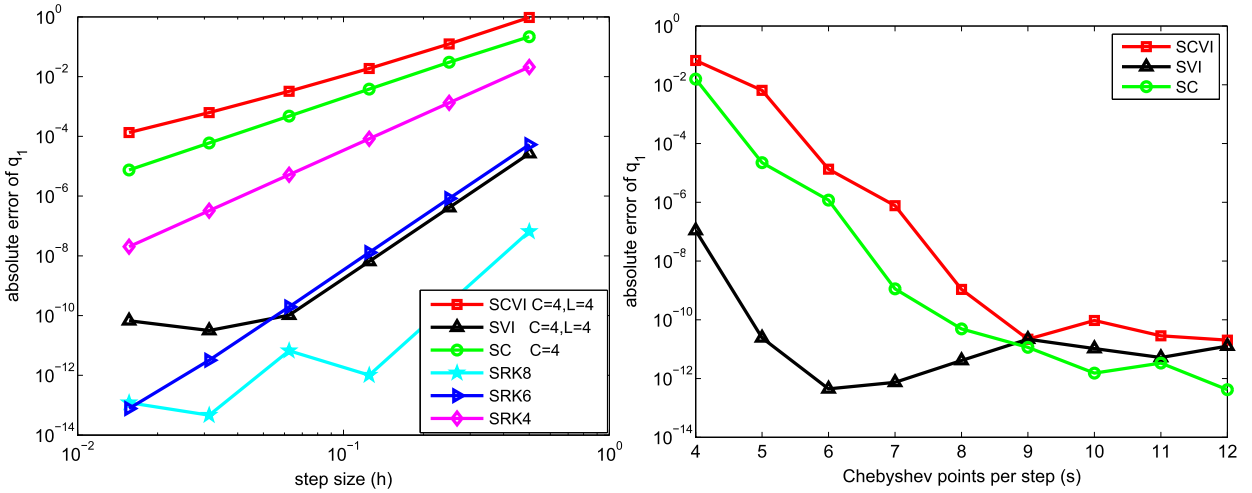

Fig. 9. Kepler two-body problem with eccentricity $e = 0$. Left: global error at $T = 20$ with h-refinement. Here, we use C in the legend to denote the number of Chebyshev points and L the number of Legendre quadrature points used to construct the method. Right: s-refinement over 100 steps of $h = 0.2$. Here, we fix the number of Legendre quadrature points to be 10.

In the left column of Fig. 6, we show the comparison of the orbits over 30 periods and in the right column of Fig. 6, the last parts of the trajectories, over one orbital period of the exact solution are given. It is clear that the period of the system does not change when using the SCVI method, but the orbital period shrinks by a factor of almost three when using the Chebyshev collocation method. In Fig. 7, we observe that the angular momentum of the Kepler two-body problem is well preserved by the SCVI, whereas the SC method exhibits a decay in the angular momentum which manifests itself very noticeably in qualitative properties of the numerical trajectory as the orbit decays dramatically. In Fig. 8, we observe a change in the orbital period in the trajectory generated by the SC method, whereas the orbital period remains much more consistent with the SCVI method. Additionally, there is a noticeable drift in the total energy, as well as the kinetic and potential energies using the SC method, whereas the SCVI method exhibits near conservation of total energy, as well as accurately tracking the energy exchange between kinetic and potential energy.

The coefficients of the Gauss–Legendre Runge–Kutta methods of various orders are given in Table 2 of [1]. It can be shown that these Gauss collocation methods are examples of symplectic Runge–Kutta methods (Section VI.4 of [4]). Fig. 9 compares the performance of SCVI with other symplectic integrators, including the spectral variational integrator (SVI), 4th-order symplectic Gauss–Legendre Runge–Kutta (SRK4) method, 6th-order symplectic Gauss–Legendre Runge–Kutta method (SRK6) and 8th-order symplectic Gauss–Legendre Runge–Kutta method (SRK8), as well as the non-symplectic spectral-

Table 1
Computational Efficiency of SC, SCVI, SVI, SRK4, SRK6, SRK8.

METHOD	SCHEME DETAIL			TOTAL TIME(s)	ERROR[a]	CPU-TIME(s)
	h	Chebyshev	Legendre			
SRK4	0.004	–	–	20	8.6973×10^{-11}	94.99
SRK6	0.05	–	–	20	5.2082×10^{-11}	16.39
SRK8	0.2	–	–	20	4.3256×10^{-11}	10.71
SC	0.2	9	–	20	1.1461×10^{-11}	0.26
SCVI	0.2	9	10	20	2.1696×10^{-11}	1.02
SVI[1]	0.2	9	10	20	2.1846×10^{-11}	5.94
SVI[2]	0.2	5	10	20	2.4120×10^{-11}	1.72

[a] absolute error of q_1

Algorithm 1 The iterative algorithm for the SCVI.

1: Choose the number of collocation points $s+1$ and the quadrature formula $(w_i, \tau_i)_{i=1}^m$.
2: Compute the differentiation matrix A, where $\tilde{A} = [a_0, A]$ is given by (12).
3: Choose the initial guess of the solution at the collocation points $Q = (q_k^1, q_k^2, ..., q_k^s)$ and v_k^0. A good initial guess for v_k^0 can be obtained by inverting the continuous Legendre transformation $p = \partial L/\partial v$.
4: Compute the right-hand sides of (19a), (19d) and their Jacobians.
5: Update $Q = (q_k^1, q_k^2, ..., q_k^s)$ and v_k^0 by performing the Newton method for (19a), (19d), until $\max(\|Q^{i+1} - Q^i\|_{\ell^\infty}, \|P^{i+1} - P^i\|_{\ell^\infty}) < TOL$, where P^i, Q^i are the value of P and Q at i-th iteration, TOL is the error tolerance.
6: Compute (q_{k+1}, p_{k+1}) by applying (19c) and (19e)
7: $k \leftarrow k+1$, repeat Step 3 to Step 6.

collocation method (SC). The numerical evidence suggests that SVI is more accurate than SCVI and SC when choosing the same number of Chebyshev points and Legendre points. We also find that the order of SCVI is almost the same as SC when using the same number of Chebyshev points, which is consistent with Theorem 2.3.

Table 1 gives the computational efficiency of SCVI when compared with SVI, SRK4, SRK6, SRK8, and SC. The comparison is inspired by the right side of Fig. 9, where SCVI, SVI and SC intersect at 9 Chebyshev points. We choose the step size, the number of Chebyshev points and the number of Legendre points differently so that the error of each method is approximately the same. It shows that the SCVI and SVI are noticeably faster than the conventional symplectic Runge–Kutta methods, even when compared to the 8-th order symplectic Gauss–Legendre Runge–Kutta method (SRK8) with the same step size. We can also see that SCVI inherits the computational efficiency of SC better than SVI. To be specific, SCVI converges faster than SVI, when they choose the same step size, the same number of Chebyshev points and the same number of Legendre points. SCVI is slightly faster than SVI for the Kepler two-body problem, even when SVI are computed with only 5 Chebyshev points. One possible explanation is that the majority of the coefficients, i.e., A, of the nonlinear equations constructed by SCVI can be calculated outside the iteration (see Algorithm 1), whereas for SVI, many coefficients of the nonlinear equations and their associated Jacobian matrices need to be recalculated with the change of q_s^i in every iteration of the Newton method [6]. This suggests that if one is interested in an efficient, high-accuracy geometric structure-preserving numerical integrator, the proposed SCVI method is a competitive choice.

In creating Table 1, we have endeavored to make the comparison fair by using the same collocation points in the SCVI and SC methods, using the same polynomial basis and quadrature rule for the SCVI and SVI methods, and using the same nonlinear solver, error norm, and termination condition for all the methods. Of course, the computational efficiency of the methods is highly implementation-dependent.

Fig. 10 presents a comparison of the orbits computed using SCVI with 10 Chebyshev points and 5, 6, 7 Gauss quadrature points from left to right. While the orbital period and phase area are accurately preserved in all three simulations, the leftmost subfigure corresponds to SCVI with 5 Gauss quadrature points and exhibits significant precession, which is why the total trajectory sweeps out an annulus. The precession is dramatically reduced as the accuracy of the quadrature method is increased. Fig. 11 presents the corresponding angular momentum and energy behaviors. From the numerical results, we see that the angular momentum and the energy error remains bounded. The accuracy of SCVI is determined by both the choice of interpolation points and quadrature points. If we fix the number of Chebyshev points, SCVI achieves higher-order accuracy as we increase the number of quadrature points, at least while the quadrature rule remains sufficiently accurate to resolve the action integral accurately.

5. Conclusions and future directions

In this paper, we provide a general method to convert any spectral-collocation method into a corresponding shooting-based variational integrator, which renders it symplectic while retaining the rate of convergence of the method. This systematically combines variational integrators with existing techniques from approximation theory, numerical quadrature and spectral methods. Another important aspect is the manner in which vectorization of the numerical method allows one to efficiently implement the spectral-collocation variational integrator. Numerical experiments demonstrate that the shooting-based variational integrators from spectral-collocation methods are symplectic, momentum-preserving and exhibit

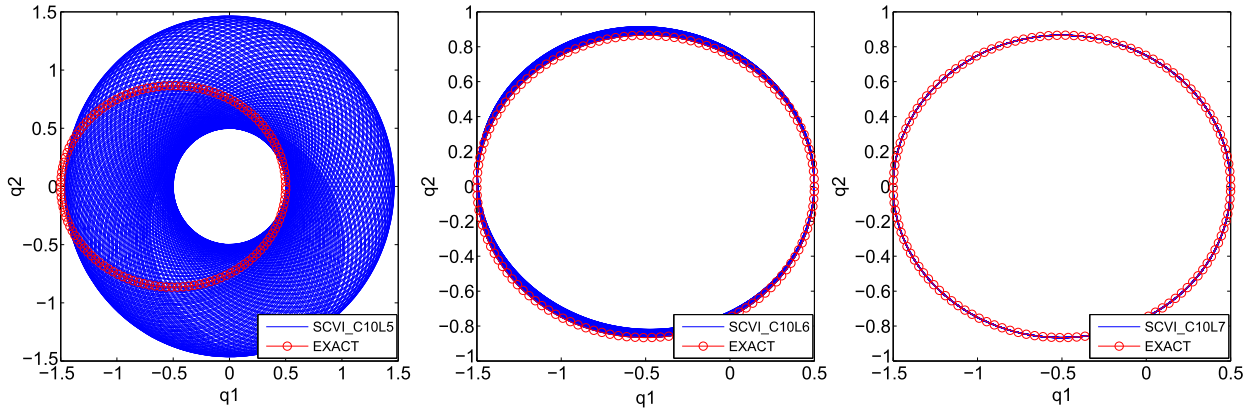

Fig. 10. Kepler two-body problem with eccentricity $e = 0.5$. Comparison of the orbit computed using SCVI with 10 point Chebyshev interpolation and 5, 6, 7 point Gauss–Legendre quadrature (from left to right). Step size $h = 0.2$ and total time $T = 400\pi$.

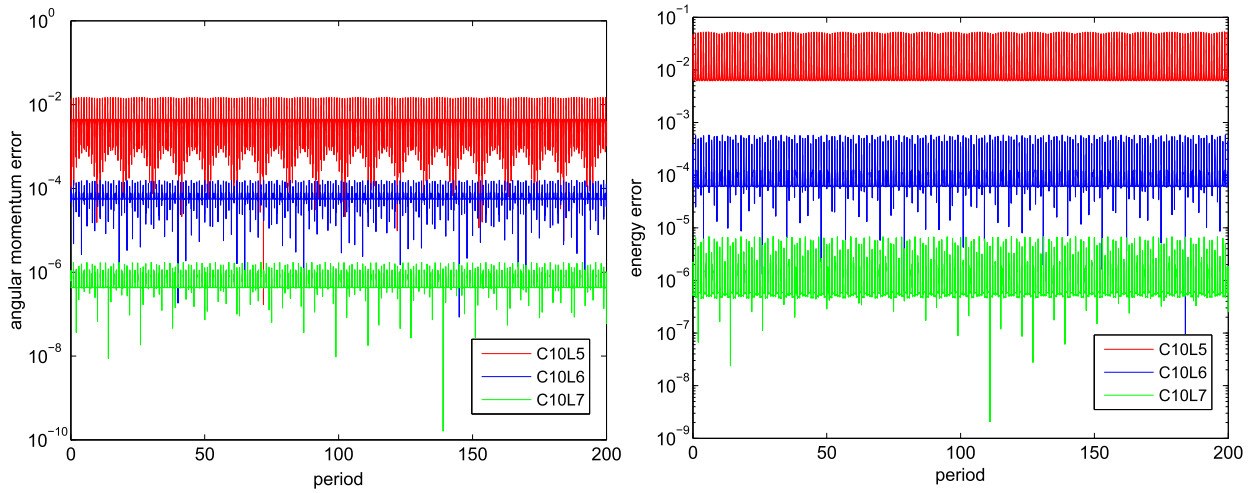

Fig. 11. Kepler two-body problem with eccentricity $e = 0.5$. Comparison of the angular momentum error and the energy error computed using SCVI with 10 point Chebyshev interpolation and 5, 6, 7 point Gauss–Legendre quadrature. Step size $h = 0.2$ and total time $T = 400\pi$. (For interpretation of the references to color in this figure, the reader is referred to the web version of this article.)

excellent energy behavior. Like its Galerkin spectral variational integrator counterpart, this new numerical method also partially inherits the computational efficiency of the underlying Chebyshev collocation method.

Spectral-collocation variational integrators are a promising option that combines computational efficiency with geometric structure-preservation. Our future work will focus on extending the synthesis of variational integrators and spectral-collocation methods to Hamiltonian PDEs and systems that evolve on Lie groups and homogeneous spaces.

Acknowledgements

The research of YQL was conducted in the mathematics department at University of California, San Diego. YQL and BYW were supported in part by the National Natural Science Foundation of China Grant No. 11271100. YQL was also supported by the short term visiting program, the graduate school of Harbin Institute of Technology. ML was supported in part by NSF Grants CMMI-1029445, DMS-1065972, CMMI-1334759, DMS-1345013, DMS-1411792, and NSF CAREER Award DMS-1010687. The authors would like to thank the referees for the helpful and constructive recommendations.

References

[1] J.C. Butcher, Implicit Runge–Kutta processes, Math. Comput. 18 (1964) 50–64.
[2] A. Farrés, J. Laskar, S. Blanes, F. Casas, J. Makazaga, A. Murua, High precision symplectic integrators for the solar system, Celest. Mech. Dyn. Astron. 116 (2) (2013) 141–174.
[3] B. Gladman, M. Duncan, J. Candy, Symplectic integrators for long-term integrations in celestial mechanics, Celest. Mech. Dyn. Astron. 52 (3) (1991) 221–240.

[4] E. Hairer, C. Lubich, G. Wanner, Structure-preserving algorithms for ordinary differential equations, in: Geometric Numerical Integration, second edition, in: Springer Series in Computational Mathematics, vol. 31, Springer-Verlag, Berlin, 2006.
[5] J. Hall, M. Leok, Spectral variational integrators, Numer. Math. 130 (4) (2015) 681–740.
[6] J. Hall, M. Leok, Lie group spectral variational integrators, Found. Comput. Math. 130 (4) (2015) 1–59.
[7] E.R. Johnson, T.D. Murphey, Scalable variational integrators for constrained mechanical systems in generalized coordinates, IEEE Trans. Robot. 25 (6) (2009) 1249–1261.
[8] N. Kanyamee, Z. Zhang, Comparison of a spectral collocation method and symplectic methods for Hamiltonian systems, Int. J. Numer. Anal. Model. 8 (1) (2011) 86–104.
[9] H.B. Keller, Numerical Methods for Two-Point Boundary Value Problems, Dover Publications, Inc., New York, 1992, Corrected reprint of the 1968 edition.
[10] M. Kobilarov, J.E. Marsden, Discrete geometric optimal control on Lie groups, IEEE Trans. Robot. 27 (4) (2011) 641–655.
[11] T. Lee, N.H. McClamroch, M. Leok, Optimal attitude control for a rigid body with symmetry, in: Proc. American Control Conf., 2007, pp. 1073–1078.
[12] M. Leok, T. Shingel, General techniques for constructing variational integrators, Front. Math. China 7 (2) (2012) 273–303.
[13] M. Leok, T. Shingel, Prolongation–collocation variational integrators, IMA J. Numer. Anal. 32 (3) (2012) 1194–1216.
[14] A. Lew, J.E. Marsden, M. Ortiz, M. West, Asynchronous variational integrators, Arch. Ration. Mech. Anal. 167 (2) (2003) 85–146.
[15] W.J. Liu, B.Y. Wu, J.B. Sun, Some numerical algorithms for solving the highly oscillatory second-order initial value problems, J. Comput. Phys. 276 (0) (2014) 235–251.
[16] J.E. Marsden, M. West, Discrete mechanics and variational integrators, Acta Numer. 10 (2001) 357–514.
[17] J.E. Marsden, S. Pekarsky, S. Shkoller, Discrete Euler–Poincaré and Lie–Poisson equations, Nonlinearity 12 (6) (1999) 1647–1662.
[18] S. Ober-Blöbaum, N. Saake, Construction and analysis of higher order Galerkin variational integrators, Adv. Comput. Math. 41 (6) (2015) 955–986.
[19] G.W. Patrick, R.J. Spiteri, W. Zhang, C. Cuell, On converting any one-step method to a variational integrator of the same order, in: 7th International Conference on Multibody Systems, Nonlinear Dynamics and Control, vol. 4, 2009, pp. 341–349.
[20] S. Reich, Backward error analysis for numerical integrators, SIAM J. Numer. Anal. 36 (5) (1999) 1549–1570.
[21] J. Timmermann, S. Khattab, S. Ober-Blöbaum, A. Trächtler, Discrete mechanics and optimal control and its application to a double pendulum on a cart, in: Proc. of the 18th IFAC World Congress, vol. 18(1), 2011, pp. 10199–10206.
[22] L.N. Trefethen, Spectral Methods in MATLAB, Software, Environments and Tools, vol. 10, Society for Industrial and Applied Mathematics (SIAM), Philadelphia, PA, 2000.